

A formulation of conserving impact system based on localized Lagrange multipliers

Y. Miyazaki^{1,*},[†] and K. C. Park²

¹ *Department of Aerospace Engineering,
College of Science and Technology, Nihon University,
7-24-1 Narashinodai, Funabashi, Chiba 274-8501, Japan*

² *Center for Aerospace Structures and
Department of Aerospace Engineering Sciences,
University of Colorado at Boulder, Campus Box 429,
Boulder, Colorado 80309-0429*

SUMMARY

This paper proposes a new finite element method of frictional impact of elastic bodies. The formulation introduces a contact frame that is placed in between contacting bodies and represents the contact surface. The non-penetration condition and the slip-stick condition are defined between the contacting body and the contact frame with the aid of the independent Lagrange multipliers representing the contact force. The position of the contact frame and the local coordinate of the contacting node along the contact frame are also treated as the independent variable, which enables the exact satisfaction of the constraint conditions without the deficiency or redundant constraint. The energy and momentum conservation algorithm is applied to the proposed impact system. In the result, the energy and the momentum is exactly conserved in case of frictionless impact. In case of frictional impact, the linear momentum is exactly conserved and the angular momentum is approximately conserved with negligible error. Copyright © 2004 John Wiley & Sons, Ltd.

KEY WORDS: contact/impact; localized Lagrange multipliers; contact frame; conservation algorithm; finite element method

1. INTRODUCTION

The numerical simulation of the contact/impact between deformable bodies has been receiving a great deal of attention in engineering field, and the remarkable progress in the computational contact/impact problem has been achieved during recent years, especially by the finite element method, and it can be observed on both the modeling and the solution method. There are two major modeling methods of the identified contact surface, the so-called master-slave

*Correspondence to: Department of Aerospace Engineering, College of Science and Technology, Nihon University, 7-24-1 Narashinodai, Funabashi, Chiba 274-8501, Japan

[†]E-mail: miyazaki@forth.aero.cst.nihon-u.ac.jp

method [1, 2, 3, 4] and interface surface method [5, 6, 7, 8, 9, 10] including the mortar element method. The problem is described with these models, and solved with the non-penetration condition. In most cases, the constraint condition is imposed by using Lagrange multipliers [3, 5, 8, 9, 10] or penalty function [2, 6, 8, 11, 12, 13, 14]. The progress has resulted in the improvement of the efficiency and the accuracy of the numerical solution.

The appropriate approximation of the contact pressure is one of the most important subjects for the accuracy of the contact analysis based on both modeling method. Several researchers have proposed the numerical methods to improve the accuracy. For example, Crisfield [3] proposed the determination method of the interpolation function of the contact force field based on the contact patch test and shown the appropriate choice of the function leads to the improvement of the accuracy. Jones and Papadopoulos [9], and Lei [10] proposed the formulation that introduces the contact pressure as the configuration variable instead of the nodal contact force, and interpolates the pressure smoothly in the interface surface. Coorevits, Hild, Pelle [15] showed the practical approximation method of statically-admissible stress field at the contact region as well as kinematically-admissible displacement field that satisfy the non-penetration condition. Several error estimator of the constitutive relation at contact region have been also proposed [7, 15].

The solution method of the non-penetration condition is also important for contact/impact problem. Traditionally, the condition is formulated at the finite element node discretely, or integral form in the contact region. Since Simo, Wriggers, and Taylor [5] proposed to solve the non-penetration condition in the weak form by the augmented Lagrangian approach based on the penalty function, and several researchers has proposed the modified methods [11, 12] to improve the accuracy without decreasing the efficiency. The augmented Lagrangian approach [6] is based on the explicit update of the value of the Lagrange multiplier, so that it is suitable for the explicit time integral scheme. This approach should, however, be employed with great care on the accuracy and convergence of the computation. The alternative approach has been proposed to improve the convergence property [13].

In case of frictional contact/impact, the problem contains the inequality constraint concerned with the frictional force. It is very difficult to ensure the existence of the solution that exactly satisfies the constitutive relation of the frictional force that is written in the inequality form. Such a difficulty does not occur in frictionless problem, i.e. it is unique to the frictional problem. This problem is still a very active research field, and several researchers have proposed the formulations and solution algorithms based on the implicit variational inequality with the penalty function [6, 8, 6, 16, 17, 18]. Rebel, Park and Felippa [19] has proposed a formulation of frictional contact problem that overcomes the numerical difficulties mentioned above. Their formulation introduces a contact frame that is similar to the conventional contact interface with one distinct difference, that is, the contact frame possesses its independent displacement degrees of freedom and its associated equilibrium equations. The equilibrium equations consist of the localized Lagrange multipliers [20]. The non-penetration condition is established between the contacting nodes and the frame, and it is satisfied exactly. The friction is taken into account between the body and the frame, instead of the contacting bodies themselves. The stick state is realized by prohibiting the slip on the frame, i.e. fixing the local coordinate of the contacting node measured on the frame. Thus the inequality associated with the frictional force is exactly satisfied. The displacement of the frame is described by those of finite number of the frame nodes. The location and the number of the frame nodes as well as the interpolation function in each frame element are determined uniquely by the contact patch test so that the obtained

pressure distribution has high accuracy [21]. The slip displacement of each contacting node is also interpolated by those of the frame nodes. The geometric bias or surface locking associated with the master-slave method [9, 22] never occurs.

The transient dynamic analysis of the contact/impact problem has the numerical difficulty other than those mentioned above. The contact/impact system is essentially a conserving system, so that the energy and momentum should be exactly conserved. However, it is not easy to ensure the conservation condition because of high nonlinearity of the system. Furthermore, the geometrically nonlinear motion with discontinuity induced by the impact cases the numerical instability in the time integral procedure. In order to clear these difficulties, the attempt to application of the so-called energy momentum method [23, 24, 25, 26, 27, 28] to the impact system has been presented for frictionless problem [29, 30, 31]. The energy momentum method modifies the equation of motion so that the conservation condition is satisfied during the impact motion. In the result, it guarantees the unconditionally stable time integration even if the motion is highly nonlinear.

The present work aims to extend the contact formulation of Rebel, Park and Felippa [19] to the dynamic case. The present formulation inherits the feature of the contact frame except the following two points. The first one is that the slip displacement of each contacting node on the frame is given as independent variable. The second one is that the frame element is separated from each other. These modification enables us to simulate the change of the contact configuration during a single time increment including the switch between contact and release state, and to avoid the singularity associated with the dependency between the unilateral contact condition and the equilibrium condition of the contact force in case of frictionless contact.

Another aim of this paper is to apply the energy momentum conservation algorithm to the contact frame formulation, and to show that the conservation condition is satisfied exactly in the frictionless impact system, and approximately in the frictional one.

The organization of this paper is as follows. In Section 3, we introduce the concept of contact frame, define the impact system based on the contact frame, and formulate the governing equations of the frictionless impact problem. In this process, we introduce the concept of partitioned frame, too. In Section 4, we apply the energy momentum conservation algorithm to the impact system defined in Section 3, and modify the governing equations. In Section 5, we extend our impact system to frictional impact problem. The solution algorithm is summarized in Section 6. We demonstrate the good performance of the formulation with the support of several examples in Section 7, and finally give the conclusion in Section 8.

2. NOTATION

In the transient impact analysis shown in the following sections, we subdivide the time domain into discrete steps of index n , and denote the time at the origin of each time step as t_n . We assume that the configuration variables at t_n are known already and those at t_{n+1} are unknowns. The time step width between t_n and t_{n+1} is denoted by Δt , i.e. $\Delta t = t_{n+1} - t_n$. We call the state at and the previous and current state, respectively.

The bar above a variable represents the averaged value of the variable at the current and the previous state. Δ represents the incremental value from the previous to the current state. We denote the value of a variable at the previous state by using the tilde under the variable,

while no index is attached to the value at the current state.

$$\bar{Z} \equiv \frac{Z(t_{n+1}) + Z(t_n)}{2}, \quad \Delta Z \equiv Z(t_{n+1}) - Z(t_n), \quad \underline{Z} \equiv Z(t_n) \quad \text{for } \forall Z \quad (1)$$

3. IMPACT SYSTEM BASED ON LOCALIZED LAGRANGE MULTIPLIERS

Let us consider the impact of two elastic bodies, body-1 and body-2, that are modeled with finite elements, and denote the domain of each body as $\Omega^{(1)}$ and $\Omega^{(2)}$, respectively. In the classical contact formulation, we determine the contacting node (slave node) and the contacted surface (master surface), and formulate the contact constraint condition between the slave nodes and the corresponding master surface. On the other hand, the present method considers the contact between the node and a curved surface located so that the two bodies are separated in opposite side as shown in Figure 1 [19]. We call this surface a contact frame, and denote its domain as Λ . The contact surface Γ is contained in the contact frame, and the equilibrium condition of the contact force acting on the contact surface will be formulated on the contact frame.

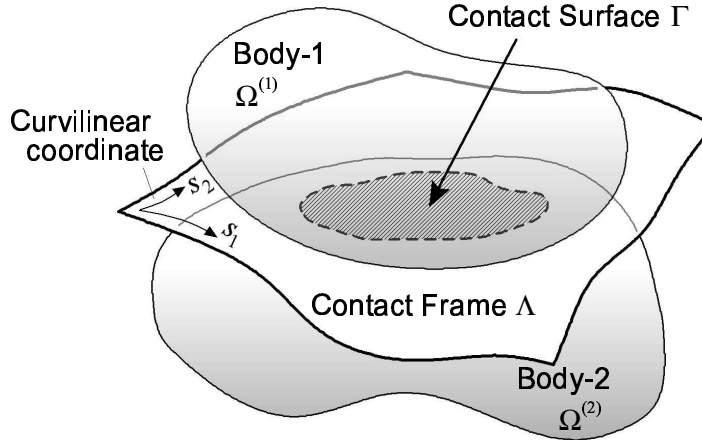


Figure 1. Contact frame

In the finite element analysis of this impact system, the contact frame is also modeled with finite elements. The initial location of the frame nodes that constitute the frame elements is determined by the contact patch test [21], which is summarized as follows. Let us consider a curvilinear coordinate system (s_1, s_2) on the contact frame Λ and define Λ^* and Γ^* as the projection of Λ and Γ on $s_1 - s_2$ plane, respectively. Then, $\Gamma^* \in \Lambda^*$ holds and the contact nodes on body-1 and body-2 can be mapped on Λ^* as in Figure 2. The frame node location on Λ^* is determined by carrying out the contact patch test on this plane. After that, the location on Λ is obtained by the inverse mapping from Λ^* to Λ . Based on the contact patch test, Rebel, Park, and Felippa [21] concluded that the frame position should be interpolated linearly by the frame nodes, i.e. the frame element should be three noded triangular or four noded quadratic

finite elements as in Figure 2.

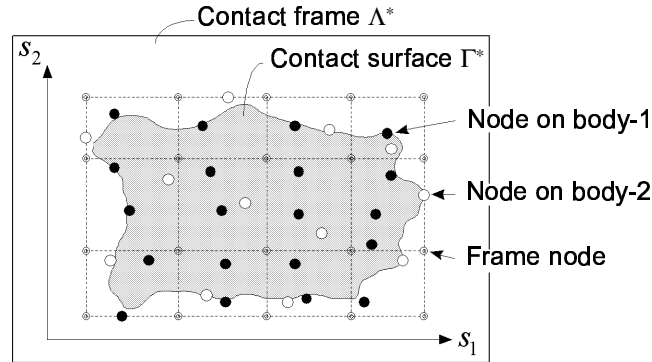


Figure 2. Placement of frame nodes

3.1. Frictionless impact problem

Let us denote the position vector of a body node on the surface of the body as \mathbf{x}_p , that of a frame node on the contact frame as \mathbf{y}_m where p and m represent the nodal number of body node and frame node, respectively. The natural coordinate (ξ_1, ξ_2) is defined on the contact frame as in Figure 3.

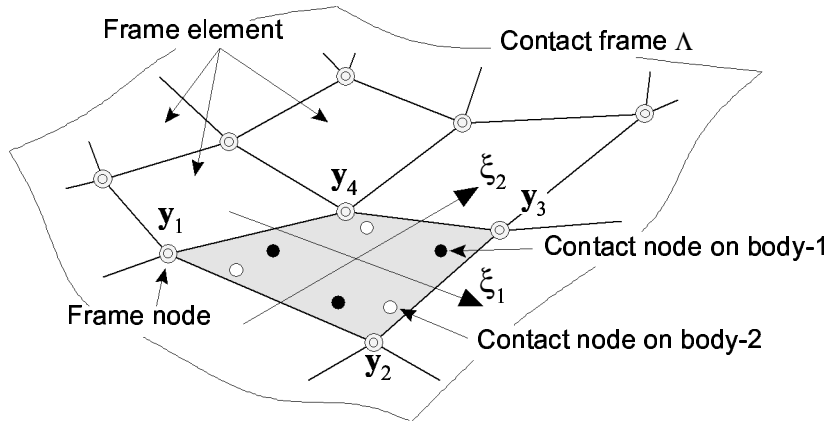


Figure 3. Frame element

In this impact system, the contact potential π_c can be defined as in Equation (2).

$$\pi_c \equiv \boldsymbol{\lambda}^p \cdot (\mathbf{x}_p - N_p^m \mathbf{y}_m) \tag{2}$$

where $\boldsymbol{\lambda}^p$ is the localized Lagrange multiplier vector that represents the contact force, and N^m is the value of the interpolation function $N^m = N^m(\xi_1, \xi_2)$ at node- p , i.e. $N_p^m = N^m(\xi_1^p, \xi_2^p)$. N_p^m has the following property.

$$\sum_m N_p^m = 1 \quad \text{for } \forall p \quad (3)$$

We can obtain the governing equation of this impact problem by applying variational principle to the total energy including π_c .

The contact condition between the body node and the contact frame is described in terms with the tangential and normal component of the contact force $\boldsymbol{\lambda}^p$ to the contact frame. Let us denote the covariant basis vector at node- p by \mathbf{g}_α^p , and the unit normal vector on the frame by \mathbf{n}^p . These are defined as Equation (4).

$$\mathbf{g}_\alpha^p = \frac{\partial N_p^m}{\partial \xi_\alpha} \mathbf{y}_m \quad , \quad \mathbf{n}^p = \eta^p \frac{\mathbf{g}_1^p \times \mathbf{g}_2^p}{|\mathbf{g}_1^p \times \mathbf{g}_2^p|} \quad \text{for } \alpha = 1, 2. \quad \forall p \quad (4)$$

where η^p is equal to 1 if the contact node hits from the negative side of the frame surface, and -1 if the positive side, i.e.

$$\eta^p = -1 \quad \text{for } p \in \Omega^{(1)} \quad , \quad \eta^p = 1 \quad \text{for } p \in \Omega^{(2)} \quad (5)$$

Then, the variation of the contact potential is written as Equation (6).

$$\delta \pi_c = (\mathbf{x}_p - N_p^m \mathbf{y}_m) \cdot \delta \boldsymbol{\lambda}^p + \boldsymbol{\lambda}^p \cdot \delta \mathbf{x}_p - (\boldsymbol{\lambda}^p \cdot \mathbf{g}_\alpha^p) \delta \xi_\alpha^p - N_p^m \delta \mathbf{y}_m \quad (6)$$

Taking into account the contact potential π_c , we obtain the governing equations (C1)-(C4) for our frictionless impact system.

$$\text{(C1)} \quad \mathbf{f}^p + \boldsymbol{\lambda}^p - \mathbf{F}^p = \mathbf{0} \quad \text{for } \forall p \quad (7)$$

$$\text{(C2)} \quad \mathbf{x}_p - N_p^m \mathbf{y}_m = \mathbf{0} \quad \text{for } \forall p \quad (8)$$

$$\text{(C3)} \quad -N_p^m \boldsymbol{\lambda}^p = \mathbf{0} \quad \text{for } \forall m \quad (9)$$

$$\text{(C4)} \quad -\mathbf{g}_\alpha^p \cdot \boldsymbol{\lambda}^p = 0 \quad \text{for } \forall p, \alpha \quad (10)$$

where \mathbf{f}^p is the nodal internal force including inertial force, and \mathbf{F}^p is the external force at node- p . The physical meanings of these equations can be summarized as follows: (C1) equilibrium of nodal force, (C2) geometrical constraint condition for the position of each contact node, (C3) momentum balance of the contact force at each frame node, and (C4) condition for frictionless contact at each contact node. The unknowns are the position vector of the body node \mathbf{x}_p , the frame node \mathbf{y}_m , the localized Lagrange multiplier vector $\boldsymbol{\lambda}^p$, and the natural coordinate ξ_α^p .

The normal component Q^p of the contact force $\boldsymbol{\lambda}^p$ to the frame surface Λ must be positive. Otherwise, the node should be released from the frame. Q^p is defined as follows.

$$Q^p = \boldsymbol{\lambda}^p \cdot \mathbf{n}^p \quad (11)$$

3.2. Partitioning of contact frame

Equations (8), (9) and (10) suggest that we can partition each frame element and formulate the governing equations for each frame element independently. The detail about the idea of the partitioning is described in this section.

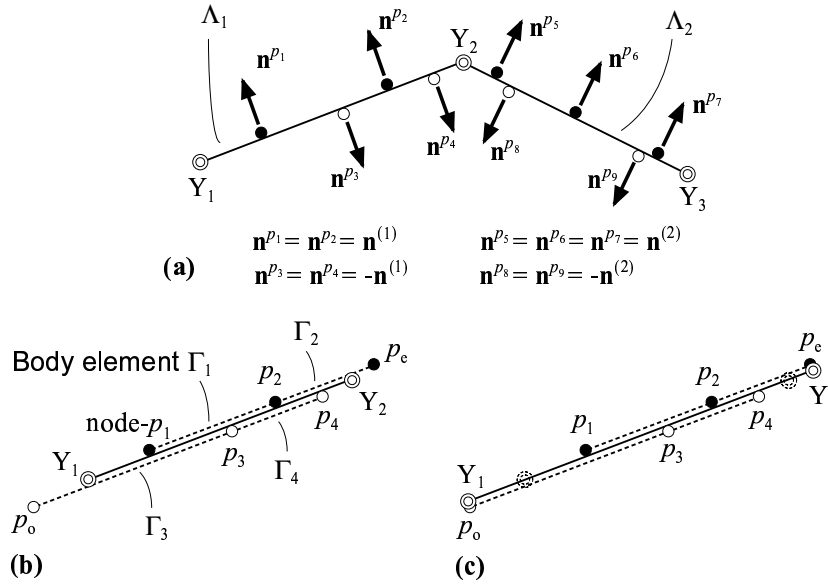


Figure 4. Geometry of contact frame in 2D case: (a) normal vector of frame element; (b) contact of body nodes and body elements; and (c) partitioned frame element

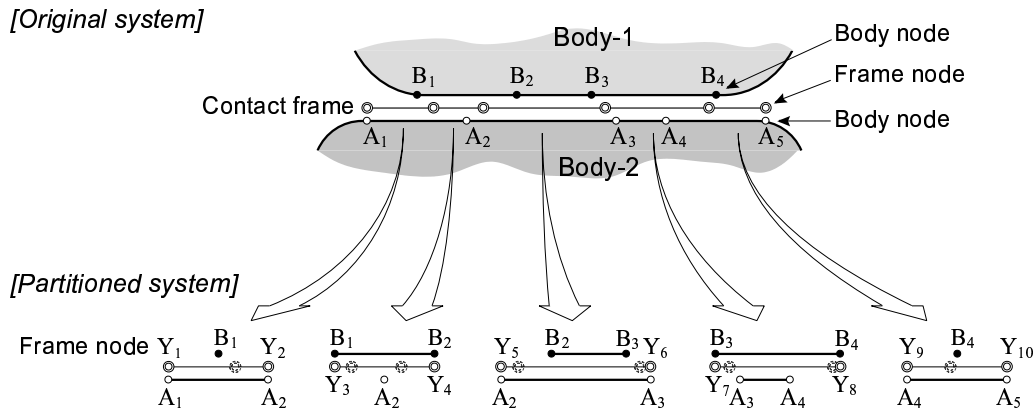


Figure 5. Partitioning of contact frame in 2D case

Let us consider 2D case of the impact system. In this case, every frame element is a straight line so that the normal vector at every contact node \mathbf{n}_p in a frame element is identical to each other. Figure 4(a) illustrates typical two frame elements, Λ_1 and Λ_2 , connected to each other. Black, white, and double circles represent the contact nodes on body-1, body-2, and frame

nodes, respectively. As shown in Figure 4(a),

$$\mathbf{n}^p = \eta^p \mathbf{n}^{(\alpha)} \quad \text{for } p \in \Lambda_\alpha, \alpha = 1, 2 \quad (12)$$

where $\mathbf{n}^{(1)}$ and $\mathbf{n}^{(2)}$ are the unit normal vector of Λ_1 and Λ_2 , respectively. Equation (10) means that the tangential component of the contact force $\boldsymbol{\lambda}^p$ vanishes. Consequently Equation (9) for the frame node Y_2 is written as Equation (13).

$$\left[\sum_{p \in \Omega(1)} N_p^{m_2} Q^p \right] \mathbf{n}^{(1)} + \left[\sum_{p \in \Omega(2)} N_p^{m_2} Q^p \right] \mathbf{n}^{(2)} = \mathbf{0} \quad (13)$$

Equation (13) is equivalent to Equation (14) if Λ_1 is not parallel to Λ_2 .

$$\sum_{p \in \Omega(1)} N_p^{m_2} Q^p = 0 \quad , \quad \sum_{p \in \Omega(2)} N_p^{m_2} Q^p = 0 \quad (14)$$

Figure 4(b) illustrates the relation between the body nodes in the frame element Λ_1 and the body elements along the boundary of each body. The body node- p_1 is in contact with body element Γ_3 , so that the body node- p_o that is out of Λ_1 should be on the line of Λ_1 . And so is the body node- p_e . This fact and Equation (14) suggest that we can partition the frame elements if each frame element is extended to involve the outer nodes such as p_o and p_e . Thus the frame element Λ_1 is partitioned and extended as Figure 4(c). In this figure, the positions of the frame node Y_1 and Y_2 are identical with those of the body node p_o and p_e , respectively. Figure 5 illustrates an example of the partitioning of contact frame.

In 3D case, the frame element can be also partitioned and extended in the same manner with 2D case. An example is shown in Figure 6. The partitioning is carried out on Λ^* . A_i are the contact nodes on body-1, and B_j are those on body-2 ($1 \leq i \leq 7$, $1 \leq j \leq 6$). A_1 , A_2 , B_1 and B_2 are included in the frame element consisting of the frame node Y_1 , Y_2 , Y_3 and Y_4 . B_1 and B_2 are in contact with the body element (A_1, A_2, A_3, A_4) and (A_2, A_5, A_6, A_7) on body-1, respectively. A_1 and A_2 are in contact with the body element (B_1, B_5, B_6, B_2) and (B_1, B_2, B_3, B_4) on body-2, respectively. Thus the frame element is partitioned and extended so that A_i and B_j are included in the element.

3.3. Consistency of partitioned contact frame

As defined in the previous subsection, a partitioned frame is a piece of a flat plane and it has unique unit normal \mathbf{n} . Let us define orthogonal basis $(\mathbf{e}_1, \mathbf{e}_2, \mathbf{n})$ on the frame (partitioned frame is called frame for simplicity hereinafter). Then, the contact equation (9) is rewritten as Equation (15).

$$N_p^m T_1^p = 0 \quad , \quad N_p^m T_2^p = 0 \quad , \quad N_p^m Q^p = 0 \quad \text{for } \forall m \quad (15)$$

where T_α^p is a tangential component of $\boldsymbol{\lambda}^p$ in the direction of \mathbf{e}_α .

$$T_\alpha^p = \boldsymbol{\lambda}^p \cdot \mathbf{e}_\alpha \quad (16)$$

Equation (10) is rewritten as (17).

$$T_\alpha^p = 0 \quad \text{for } \forall p, \alpha \quad (17)$$

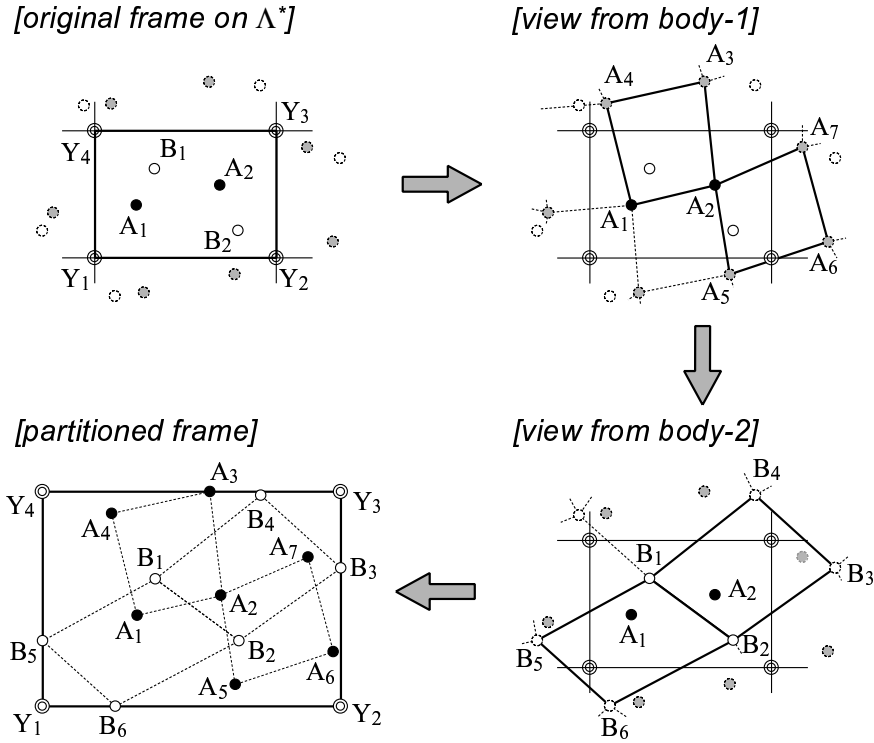


Figure 6. Partitioning of frame element in 3D case

The first and second equations of Equation (15) are unconditionally satisfied if Equation (17) holds. Furthermore, Equation (15) and (8) allow arbitrary rigid displacement of the frame node in the contact plane Λ^* . Thus Equation (8), (15) and (17) are not independent to each other, so that the solution of these equations has indeterminacy. If the frame consists of four or more noded element, there are the additional constraints for the position of the frame nodes that the nodes are located on a plane at the current state as well as the previous state (These constraints are automatically satisfied if the frame consists of three noded triangular element).

In order to avoid this indeterminacy and to satisfy the additional constraint, we enforce the following two conditions as well as the condition that all frame nodes are on a plane at the previous state.

(C5) The motion of the frame from the previous to the current state must be a rigid one, and the axis of the rigid rotation is parallel to the frame plane at the previous state as in Figure 7. In 3D case, the total number of the condition is $(3n_f - 5)$ where n_f is the number of frame nodes. The total number is 1 in 2D case.

(C6) The natural coordinate (ξ_1^p, ξ_2^p) of a specific contact node is fixed, i.e. these values at the current state are the same as those at the previous state. The

node located at the boundary of the partitioned frame is suitable to be fixed. The number of this condition is 2 in 3D case, and 1 in 2D case.

Thus the total number of these enforced conditions, n_c , is

$$n_c = \begin{cases} 3n_f - 3 & \text{in 3D case} \\ 2 & \text{in 2D case} \end{cases} \quad (18)$$

Therefore, we replace n_c equations in the frictionless contact condition (C4) with (C5) and (C6). This replacement makes the governing equation independent to each other, so that we can solve the problem without any indeterminacy.

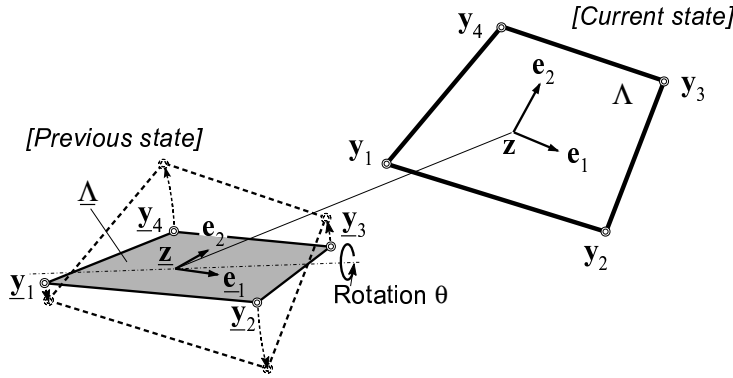


Figure 7. Rigid motion of partitioned frame

The implementation procedure of the constraint condition (C5) is summarized in the followings.

In 3D case, the constraint condition (C5) can be implemented by introducing five new configuration variables, too. When the frame is constructed at the previous state, the frame node position is expressed as follows.

$$\underline{\mathbf{y}}_m = \underline{\mathbf{z}} + \underline{s}_\alpha^m \underline{\mathbf{e}}_\alpha \quad \text{for } \forall m \quad (19)$$

where $\underline{\mathbf{e}}_\alpha$ ($\alpha = 1, 2$) is the orthogonal basis vector tangential to the frame plane $\underline{\Delta}$ at the previous state, and \underline{s}_α^m is the coordinate of the frame node- m on $\underline{\Delta}$. Then, (C5) requires that the frame node position is described in terms with two vectors $\underline{\mathbf{z}}$ and $\boldsymbol{\theta}$ as Equation (20).

$$\mathbf{y}_m = \mathbf{z} + \underline{s}_\alpha^m \mathbf{R}(\boldsymbol{\theta}) \underline{\mathbf{e}}_\alpha \quad (20)$$

where $\mathbf{R}(\boldsymbol{\theta})$ is the rotation matrix described by the finite rotation vector $\boldsymbol{\theta}$. $\boldsymbol{\theta}$ is parallel to the axis of the rotation. \mathbf{z} and $\boldsymbol{\theta}$ are expressed as

$$\mathbf{z} = (z_1, z_2, z_3)^T, \quad \boldsymbol{\theta} = \theta_\alpha \underline{\mathbf{e}}_\alpha \quad (21)$$

Thus the five independent variables ($z_1, z_2, z_3, \theta_1, \theta_2$) are necessary to describe the frame node position. The total number of Equation (20) is $3n_f$. In the result, we can solve our impact system by removing $(3n_f - 5)$ equations in (C4) and implementing Equation (20).

It is also possible to implement (C5) without introducing new variable. For example, (C5) is expressed as Equation in case that the frame is four noded quadratic element ($n_f = 4$ and the number of condition (C5) is seven).

$$\begin{aligned} |\mathbf{y}_2 - \mathbf{y}_1| - |\underline{\mathbf{y}}_2 - \underline{\mathbf{y}}_1| &= 0, & |\mathbf{y}_3 - \mathbf{y}_2| - |\underline{\mathbf{y}}_3 - \underline{\mathbf{y}}_2| &= 0, & |\mathbf{y}_4 - \mathbf{y}_3| - |\underline{\mathbf{y}}_4 - \underline{\mathbf{y}}_3| &= 0, \\ |\mathbf{y}_1 - \mathbf{y}_4| - |\underline{\mathbf{y}}_1 - \underline{\mathbf{y}}_4| &= 0, & |\mathbf{y}_3 - \mathbf{y}_1| - |\underline{\mathbf{y}}_3 - \underline{\mathbf{y}}_1| &= 0, & |\mathbf{y}_4 - \mathbf{y}_2| - |\underline{\mathbf{y}}_4 - \underline{\mathbf{y}}_2| &= 0, \\ (\bar{\mathbf{y}}_2 - \bar{\mathbf{y}}_1) \cdot (\Delta \mathbf{y}_4 - \Delta \mathbf{y}_1) &= 0 \end{aligned} \quad (22)$$

In case of 2D impact, (C5) is expressed as Equation (23) for example.

$$|\mathbf{y}_2 - \mathbf{y}_1| - |\underline{\mathbf{y}}_2 - \underline{\mathbf{y}}_1| = 0 \quad (23)$$

4. ENERGY MOMENTUM CONSERVATION PROCEDURE

The governing equations (7)-(10) can be solved with given time integral scheme. However, the total energy and momentum may not be conserved unless appropriate conservation algorithm is employed. Impact is essentially a conservative problem, i.e. the linear and angular momentum are conserved and the total energy is also conserved if the impact is perfectly elastic and frictionless. Numerical analysis of impact system should satisfy this conservation condition to provide highly accurate results and stable time integration.

In this paper, we propose to apply the energy momentum method [23, 24, 25, 26, 27] to our impact system. The energy momentum method ensures the preservation of total energy and momentum, and is a quite powerful method for the analysis of highly nonlinear elastodynamic system. The application of this method to the impact system based on the contact frame is described in the following subsections.

4.1. Modified equation of motion

Firstly, let us consider a non-contact system, and denote the linear momentum by \mathbf{P} , the angular momentum by \mathbf{L} , and the total energy of the bodies including the kinetic energy, strain energy, and other internal energy by π . The energy momentum method requires the modified nodal force vector $\tilde{\mathbf{f}}^p$ satisfying Equation (24) and (25).

$$\Delta \pi = \tilde{\mathbf{f}}^p \cdot \Delta \mathbf{x}_p \quad (24)$$

$$\frac{\Delta \mathbf{P}}{\Delta t} = \tilde{\mathbf{f}}^p, \quad \frac{\Delta \mathbf{L}}{\Delta t} = \bar{\mathbf{x}}^p \times \tilde{\mathbf{f}}^p \quad (25)$$

$$(26)$$

Based on the energy-momentum method, the equation of motion for the non-contact system is given as follows.

$$\tilde{\mathbf{f}}^p - \bar{\mathbf{F}}^p = \mathbf{0} \quad \text{for } \forall p \quad (27)$$

Equation (27) is solved with the following time integration scheme.

$$\frac{\Delta \mathbf{x}^p}{\Delta t} = \bar{\dot{\mathbf{x}}}^p \quad (28)$$

where $\dot{\mathbf{x}}^p$ is the velocity vector at node- p . When Equation (27) and (28) are solved simultaneously, we obtain that

$$\Delta\pi = \Delta\mathbf{x}_p \cdot \bar{\mathbf{F}}^p \quad (29)$$

$$\frac{\Delta\mathbf{P}}{\Delta t} = \bar{\mathbf{F}}^p \quad , \quad \frac{\Delta\mathbf{L}}{\Delta t} = \bar{\mathbf{x}}^p \times \bar{\mathbf{F}}^p \quad (30)$$

Equation (29) and (30) show that the conservation principles of the energy and momentum are satisfied approximately, and the total energy and momentum are conserved exactly if there is no external force.

In our impact system, the total energy is the summation of the energy stored in the bodies and the contact potential.

$$\pi^* = \pi + \pi_c \quad (31)$$

From Equation (2) and (24), we obtain the incremental expression of π^* as

$$\begin{aligned} \Delta\pi^* = & (\tilde{\mathbf{f}}^p + \bar{\boldsymbol{\lambda}}^p) \cdot \Delta\mathbf{x}_p + (\bar{\mathbf{x}}_p - \overline{N_p^m \mathbf{y}_m}) \cdot \Delta\boldsymbol{\lambda}^p \\ & + (\overline{N_p^m} \bar{\boldsymbol{\lambda}}^p) \cdot \Delta\mathbf{y}_m - \left(\frac{\delta N_p^m}{\delta \xi_\alpha^p} \bar{\mathbf{y}}_m \cdot \bar{\boldsymbol{\lambda}}^p \right) \Delta\xi_\alpha^p \end{aligned} \quad (32)$$

where $\delta N_p^m / \delta \xi_\alpha^p$ is determined so as to satisfy Equation (33).

$$\Delta N_p^m = \sum_{\beta=1}^2 \left[\frac{\delta N_p^m}{\delta \xi_\beta^p} \right] \Delta\xi_\beta^p \quad , \quad \lim_{\Delta t \rightarrow 0} \frac{\delta N_p^m}{\delta \xi_\alpha^p} = \frac{\partial N_p^m}{\partial \xi_\alpha^p} \quad \text{for } \forall m, p, \alpha \quad (33)$$

From Equation (32), we can obtain the modified governing equation in case of frictionless impact like Equations (7)-(10).

$$(C1)' \quad \tilde{\mathbf{f}}^p + \bar{\boldsymbol{\lambda}}^p - \bar{\mathbf{F}}^p = \mathbf{0} \quad \text{for } \forall p \quad (34)$$

$$(C2)' \quad \bar{\mathbf{x}}_p - \overline{N_p^m \mathbf{y}_m} = \mathbf{0} \quad , \quad \tilde{Q}^p > 0 \quad \text{for } \forall p \quad (35)$$

$$(C3)' \quad -\overline{N_p^m} \bar{\boldsymbol{\lambda}}^p = \mathbf{0} \quad \text{for } \forall m \quad (36)$$

$$(C4)' \quad -\tilde{\mathbf{g}}_\alpha^p \cdot \bar{\boldsymbol{\lambda}}^p = 0 \quad \text{for } \forall p, \alpha \quad (37)$$

where \tilde{Q}^p is the normal component of the contact force $\bar{\boldsymbol{\lambda}}^p$, and $\tilde{\mathbf{g}}_\alpha^p$ is the tangential vector of $\bar{\boldsymbol{\lambda}}$ defined as Equation (38).

$$\tilde{\mathbf{g}}_\alpha^p = \frac{\delta N_p^m}{\delta \xi_\alpha^p} \bar{\mathbf{y}}_m \quad (38)$$

Equation (37) suggests that $\tilde{\mathbf{g}}_\alpha^p$ is tangential to the contact surface, i.e. $\bar{\boldsymbol{\lambda}}$ is the equivalent slip surface of our discretized impact problem. The unit normal vector of the equivalent slip surface is defined as Equation (39).

$$\tilde{\mathbf{n}}^p = \eta^p \frac{\tilde{\mathbf{g}}_1^p \times \tilde{\mathbf{g}}_2^p}{|\tilde{\mathbf{g}}_1^p \times \tilde{\mathbf{g}}_2^p|} \quad (39)$$

Thus \tilde{Q}^p is defined as

$$\tilde{Q}^p = \bar{\boldsymbol{\lambda}}^p \cdot \tilde{\mathbf{n}}^p \quad (40)$$

Equation (35).1 has a serious problem on the geometry of the frame. If node- p is not on the frame at the previous time state, $\underline{\mathbf{x}}_p$ can be expressed as

$$\underline{\mathbf{x}}_p = \underline{N}_p^m \underline{\mathbf{y}}_m + \underline{\Delta}_p \underline{\mathbf{n}}_p \quad (41)$$

where $\underline{\Delta}_p$ is the distance between node- p and the frame at the previous state, and $\underline{\Delta}_p < 0$. Then, Equation(35).1 results in

$$\underline{\mathbf{x}}_p - N_p^m \underline{\mathbf{y}}_m = -(\underline{\mathbf{x}}_p - \underline{N}_p^m \underline{\mathbf{y}}_m) = -\underline{\Delta}_p \underline{\mathbf{n}}_p \neq \mathbf{0} \quad (42)$$

Equation (42) means that the contact condition is not satisfied, i.e. node- p is not on the frame at the current time state, which is not acceptable in view of the accuracy of impact analysis. Therefore, we should modify Equation(35).1 so that the contact condition is satisfied without the violation of the conservation conditions. Let us modify Equation(35) as follows.

$$(C2)' \quad \frac{1}{2} (\underline{\mathbf{x}}_p - N_p^m \underline{\mathbf{y}}_m - \underline{\Delta}_p \underline{\mathbf{w}}^p) = \mathbf{0}, \quad \tilde{Q}^p > 0 \quad \text{for } \forall p \quad (43)$$

Then, Equation (43) is geometrically admissible if Equation (44) holds.

$$\underline{\mathbf{w}}^p \cdot \underline{\mathbf{n}}^p = \mathbf{0} \quad \text{for } \forall p \quad (44)$$

In the next subsection, $\underline{\mathbf{w}}^p$ will be determined so that the conservation of the momentum is satisfied.

4.2. Conservation of momentum

Taking into account that Equation (25) holds, we obtain the increment of the momentum in our impact system as Equation (45) by solving (C1').

$$\frac{\Delta \mathbf{P}}{\Delta t} = \bar{\mathbf{F}}^p - \bar{\boldsymbol{\lambda}}^p \quad (45)$$

$$\frac{\Delta \mathbf{L}}{\Delta t} = \bar{\mathbf{x}}_p \times \bar{\mathbf{F}}^p - \bar{\mathbf{x}}_p \times \bar{\boldsymbol{\lambda}}^p \quad (46)$$

The conservation principle of the momentum requires that the second terms of the right side of these equations vanish. Equation (36) and (3) ensure the conservation of the linear momentum as shown in Equation (47).

$$\sum_p \bar{\boldsymbol{\lambda}}^p = \sum_m \sum_p \bar{N}_p^m \bar{\boldsymbol{\lambda}}^p = \mathbf{0} \quad (47)$$

As mentioned in the previous subsection, the vector $\underline{\mathbf{w}}^p$ is determined by the conservation principle of the angular momentum, which is shown in the rest of this subsection.

The conservation condition of the angular momentum is

$$\bar{\mathbf{x}}_p \times \bar{\boldsymbol{\lambda}}^p = \mathbf{0} \quad (48)$$

By using Equation (43), the conservation condition is rewritten as

$$\bar{N}_p^m \underline{\mathbf{y}}_m \times \bar{\boldsymbol{\lambda}}^p + \left(\underline{\Delta}_p \frac{\underline{\mathbf{w}}^p + \underline{\mathbf{n}}^p}{2} \right) \times \bar{\boldsymbol{\lambda}}^p = \mathbf{0} \quad (49)$$

As shown in Equation (19) and (20), $\underline{\mathbf{y}}_m$, \mathbf{y}_m , and $\bar{\mathbf{y}}_m$ are located on planes extended with $\underline{\mathbf{e}}_\alpha$, \mathbf{e}_α , and $\bar{\mathbf{e}}_\alpha$, respectively.

$$\underline{\mathbf{y}}_m = \underline{\mathbf{z}} + \underline{s}_\alpha^m \underline{\mathbf{e}}_\alpha \quad , \quad \mathbf{y}_m = \mathbf{z} + s_\alpha^m \mathbf{e}_\alpha \quad , \quad \bar{\mathbf{y}}_m = \bar{\mathbf{z}} + \underline{s}_\alpha^m \bar{\mathbf{e}}_\alpha \quad (50)$$

Let us denote the normal vector of the frame plane $\underline{\Lambda}$, Λ , and $\bar{\Lambda}$ by $\underline{\mathbf{n}}$, \mathbf{n} , and $\bar{\mathbf{n}}$, respectively.

$$\underline{\mathbf{n}} \equiv \frac{\underline{\mathbf{e}}_1 \times \underline{\mathbf{e}}_2}{|\underline{\mathbf{e}}_1 \times \underline{\mathbf{e}}_2|} \quad , \quad \mathbf{n} \equiv \frac{\mathbf{e}_1 \times \mathbf{e}_2}{|\mathbf{e}_1 \times \mathbf{e}_2|} \quad , \quad \bar{\mathbf{n}} \equiv \frac{\bar{\mathbf{e}}_1 \times \bar{\mathbf{e}}_2}{|\bar{\mathbf{e}}_1 \times \bar{\mathbf{e}}_2|} \quad (51)$$

Then, the requirement that the rotation axis of the orthogonal basis is parallel to $\underline{\Lambda}$ leads to the following relations.

$$\bar{\mathbf{e}}_1 \cdot \Delta \mathbf{e}_2 = \bar{\mathbf{e}}_2 \cdot \Delta \mathbf{e}_1 = 0 \quad , \quad \Delta \mathbf{e}_1 \times \bar{\mathbf{n}} = \Delta \mathbf{e}_2 \times \bar{\mathbf{n}} = \mathbf{0} \quad , \quad \bar{\mathbf{n}} = \frac{\bar{\mathbf{n}}}{|\bar{\mathbf{n}}|} \quad , \quad \Delta \mathbf{n} \cdot \bar{\mathbf{n}} = 0 \quad (52)$$

Considering these relations, we can prove that the first term of the left side of Equation (49) is $\mathbf{0}$ as follows. Let us denote the orthogonal basis vectors parallel to $\bar{\Lambda}$ by $\tilde{\mathbf{e}}_\alpha$, and express the contact force $\bar{\boldsymbol{\lambda}}^p$ in component fashion.

$$\bar{\boldsymbol{\lambda}}^p = \eta^p \tilde{Q}^p \bar{\mathbf{n}} + \tilde{T}_\alpha^p \tilde{\mathbf{e}}_\alpha \quad (53)$$

\tilde{T}_α^p represents the tangential component of the contact force. The frictionless contact condition (C4)' is equivalent to Equation (54).

$$\bar{\boldsymbol{\lambda}}^p = \eta^p \tilde{Q}^p \bar{\mathbf{n}} \quad , \quad \tilde{T}_\alpha^p = 0 \quad \text{for } \forall p, \alpha \quad (54)$$

Under this condition, the momentum equilibrium condition (C3)' is equivalent to Equation (55)

$$\bar{N}_p^m \eta^p \tilde{Q}^p = 0 \quad \text{for } \forall m \quad (55)$$

By the substitution of Equation (50) and (54), the first term of the left side of Equation (49) is recalculated as follows.

$$\begin{aligned} \overline{N_p^m \mathbf{y}_m} \times \bar{\boldsymbol{\lambda}}^p &= \left(\bar{N}_p^m \bar{\mathbf{y}}_m + \frac{1}{4} \Delta N_p^m \Delta \mathbf{y}_m \right) \times \eta^p \tilde{Q}^p \bar{\mathbf{n}} \\ &= \left(\bar{N}_p^m \eta^p \tilde{Q}^p \right) \bar{\mathbf{y}}_m \times \bar{\mathbf{n}} + \frac{1}{4} \Delta N_p^m \left(\Delta \mathbf{z} \times \eta^p \tilde{Q}^p \bar{\mathbf{n}} \right) + \frac{1}{4} \Delta N_p^m s_\alpha^m \eta^p \tilde{Q}^p (\Delta \mathbf{e}_\alpha \times \bar{\mathbf{n}}) \end{aligned} \quad (56)$$

Using Equations (3), (52) and (55), we conclude that the right hand of Equation (56) is $\mathbf{0}$.

Considering Equation (52), we conclude that Equation (49) is satisfied by defining \mathbf{w}^p as Equation (57).

$$\mathbf{w}^p \equiv \mathbf{n}^p - \frac{1}{\bar{\mathbf{n}}^p \cdot \mathbf{n}^p} \bar{\mathbf{n}}^p = \eta^p \left(\mathbf{n} - \frac{1}{\bar{\mathbf{n}} \cdot \mathbf{n}} \bar{\mathbf{n}} \right) \quad (57)$$

Thus we can conclude that the conservation principle of the momentum,(30), is satisfied by solving Equations (34), (43), (36), and (37) with the time integral scheme (28).

4.3. Conservation of energy

The increment of the body energy in this impact system is recalculated as Equation (58) by using Equation (24) and (34).

$$\Delta\pi = \Delta\mathbf{x}_p \cdot \bar{\mathbf{F}}^p - \Delta\pi_c \quad (58)$$

where

$$\Delta\pi_c = \Delta\mathbf{x}_p \cdot \bar{\boldsymbol{\lambda}}^p \quad (59)$$

By substituting Equation (41) and (43) into (59), we obtain

$$\Delta\pi_c = [\Delta N_p^m \bar{\mathbf{y}}_m + \bar{N}_p^m \Delta \mathbf{y}_m + \underline{\Delta}_p (\mathbf{w}^p - \underline{\mathbf{n}}^p)] \cdot \bar{\boldsymbol{\lambda}}^p \quad (60)$$

Equation (36), (37), (52), and (57) lead the following relations.

$$\Delta N_p^m \bar{\mathbf{y}}_m \cdot \bar{\boldsymbol{\lambda}}^p = 0 \quad , \quad \bar{N}_p^m \Delta \mathbf{y}_m \cdot \bar{\boldsymbol{\lambda}}^p = 0 \quad , \quad \mathbf{w}^p - \underline{\mathbf{n}}^p = \eta^p \left(\Delta \mathbf{n} - \frac{1}{\tilde{\mathbf{n}} \cdot \mathbf{n}} \tilde{\mathbf{n}} \right) \quad (61)$$

By substituting Equation (61) and the fourth equation of (52) into (60), we conclude

$$\Delta\pi_c = -\frac{\underline{\Delta}_p \tilde{Q}^p}{\tilde{\mathbf{n}} \cdot \mathbf{n}} \quad (62)$$

$\Delta\pi_c$ is positive because $\underline{\Delta}_p$ is negative and \tilde{Q}^p is positive. In order to achieve the conservation of the body energy, we will introduce *the discrete contact velocity* in the following section.

4.4. Discrete contact velocity

The idea of *discrete contact velocity* has been proposed in reference [31]. This idea requires a discrete jump of the velocity after the governing equations (34), (43), (36) and (37) are solved. Let us denote the current velocity obtained from the governing equations by $\dot{\mathbf{x}}_*^p$, and modify the current velocity by adding the discrete contact velocity \mathbf{v}_c^p , i.e.

$$\dot{\mathbf{x}}^p = \dot{\mathbf{x}}_*^p + \mathbf{v}_c^p \quad (63)$$

This velocity jump causes the jump of the energy and momentum as in Equation (64).

$$\begin{aligned} \left(\frac{\Delta \mathbf{P}}{\Delta t} \right)_{jump} &= M_{pq} \frac{\mathbf{v}_c^q}{\Delta t} \\ \left(\frac{\Delta \mathbf{L}}{\Delta t} \right)_{jump} &= \mathbf{x}_p \times M_{pq} \frac{\mathbf{v}_c^q}{\Delta t} \\ (\Delta \pi)_{jump} &= \frac{1}{2} M_{pq} \mathbf{v}_c^p \cdot \mathbf{v}_c^q + M_{pq} \dot{\mathbf{x}}_*^p \cdot \mathbf{v}_c^q \end{aligned} \quad (64)$$

where M_{pq} is the component of mass matrix contributed by node- p and node- q .

After the governing equations are solved, the energy decreases of the amount $\Delta\pi_c$. Therefore, our purpose is to find \mathbf{v}_c^q that satisfies the conservation conditions, i.e. the following relations.

$$\left(\frac{\Delta \mathbf{P}}{\Delta t} \right)_{jump} = \mathbf{0} \quad , \quad \left(\frac{\Delta \mathbf{L}}{\Delta t} \right)_{jump} = \mathbf{0} \quad , \quad (\Delta \pi)_{jump} = \Delta\pi_c \quad (65)$$

Let us define \mathbf{v}_c^q as Equation (66) so that the first conservation condition of Equation (65) is satisfied automatically.

$$M_{pq} \frac{\mathbf{v}_c^q}{\Delta t} = a_m \bar{N}_p^m \eta^p \tilde{Q}^p \tilde{\mathbf{n}} \quad \text{for } \forall p \quad (66)$$

where a_m is the parameter determined later. Substituting Equation (66) into the second equation of (65), we obtain

$$\left(\frac{\Delta \mathbf{L}}{\Delta t} \right)_{jump} = a_m w_\alpha^m \tilde{\mathbf{e}}_\alpha \quad (67)$$

where

$$w_\alpha^m = \bar{N}_p^m \eta^p \tilde{Q}^p (\mathbf{x}_p \times \tilde{\mathbf{n}}) \cdot \tilde{\mathbf{e}}_\alpha \quad (68)$$

The conservation condition of the angular momentum, i.e. the second equation of (65), is automatically satisfied if Equation (69) holds.

$$a_m w_1^m = a_m w_2^m = 0 \quad (69)$$

This equation has non-zero solution for a_m (The relation $m \geq 3$ holds in case of 3D impact. The relations $w_2^m = 0$ and $m \geq 2$ hold in case of 2D impact. Therefore, there exists non-zero solution). Let us denote the solution as

$$a_m = b^{(i)} a_m^{(i)} \quad (70)$$

where (i) represents the frame element number in which the frame node- m is involved, and $a_m^{(i)}$ is the solution of (69). Then, Equation (66) is rewritten as follows.

$$\mathbf{v}_c^p = b^{(i)} \mathbf{u}_p^{(i)} \quad , \quad \mathbf{u}_p^{(i)} \equiv a_m^{(i)} [M_{pq}]^{-1} \bar{N}_q^m \eta^q \tilde{Q}^q \tilde{\mathbf{n}}^{(i)} \Delta t \quad (71)$$

Substituting this equation into the third equation of Equation (65), we obtain a nonlinear equation for $b^{(i)}$.

$$A_{ij} b^{(i)} b^{(j)} + B_i b^{(i)} - \Delta \pi_c = 0 \quad (72)$$

where

$$A_{ij} = \frac{1}{2} M_{pq} \mathbf{u}_p^{(i)} \cdot \mathbf{u}_q^{(j)} \quad , \quad B_i = M_{pq} \dot{\mathbf{x}}_*^p \cdot \mathbf{u}_q^{(i)} \quad (73)$$

We can obtain the solution of (72) by iterative procedure such as Newton-Raphson method. Since $\Delta \pi_c$ has very small positive value, Equation (72) has non-zero unique solution that satisfies

$$b^{(i)} = \frac{-B'_i + \text{sgn}(B_i) \sqrt{(B'_i)^2 + 4A_{ii} \Delta \pi_c}}{2A_{ii}} \quad (74)$$

where

$$B'_i = B_i + \sum_{j \neq i} A_{ij} b^{(j)} \quad (75)$$

After $b^{(i)}$ is obtained, the velocity at the current state that satisfies the conservation condition is calculated by using Equation (63) and (71).

Thus we solve the impact system by two stages. The first stage is to solve the governing equations of the impact system, (34), (43), (36) and (37), with the time integration scheme (28). The second stage is to add the discrete contact velocity \mathbf{v}_c^p to the obtained velocity.

5. FRICTIONAL IMPACT

In case that there is Coulomb friction between two bodies, we should consider the frictional force acting between the body nodes and the frame. In this section, we extend our formulation to the frictional impact problem.

The frictional force \tilde{T}^p is defined as the tangential component of the contact force $\bar{\lambda}^p$ to the slip surface $\bar{\Lambda}$.

$$\tilde{T}^p \equiv \sqrt{(\tilde{T}_1^p)^2 + (\tilde{T}_2^p)^2} = |\bar{\lambda}^p \times \tilde{\mathbf{n}}| \quad (76)$$

When the body node is in the slip state, the frictional force should be in the opposite direction of the slip displacement. The slip displacement \mathbf{u}_p and the unit vector $\tilde{\mathbf{e}}_{fr}^p$ along the slip displacement is written as Equation (77).

$$\tilde{\mathbf{e}}_{fr}^p = \frac{\mathbf{u}_p}{|\mathbf{u}_p|} \quad , \quad \mathbf{u}_p = \Delta N_p^m \bar{\mathbf{y}}_m \quad (77)$$

Let Γ_{slip} and Γ_{stick} denote the set of contact nodes that are in the slip state and the stick state, respectively.

$$\Gamma_{slip} \equiv \{p | p \in \underline{\Gamma}, \tilde{T}^p > \mu \tilde{Q}^p\} \quad , \quad \Gamma_{stick} \equiv \{p | p \in \underline{\Gamma}, \tilde{T}^p \leq \mu \tilde{Q}^p\} \quad (78)$$

Then, we can simulate the frictional impact problem by replacing the governing equation (37) with (79).

$$(C4)' \quad \begin{cases} \tilde{\mathbf{e}}_\alpha \cdot [\mu \tilde{Q}^p \tilde{\mathbf{e}}_{fr}^p - \bar{\lambda}^p] = 0 & \text{if } p \in \Gamma_{slip} \\ \frac{\xi_\alpha^p - \xi_\alpha^{\min}}{\xi_\alpha^{\max} - \xi_\alpha^{\min}} = \frac{\xi_\alpha^p - \xi_\alpha^{\min}}{\xi_\alpha^{\max} - \xi_\alpha^{\min}} & \text{if } p \in \Gamma_{stick} \end{cases} \quad (79)$$

It must be noted that this modification guarantees the conservation of the linear momentum. The angular momentum is not conserved exactly, but it has a very small amount of the deviation as in Equation (80).

$$\frac{\Delta \mathbf{L}}{\Delta t} = \left[\frac{1}{4} \Delta N_p^m (\Delta \mathbf{y}_m \cdot \tilde{\mathbf{n}}) + \eta^p \underline{\Delta}_p \left(|\tilde{\mathbf{n}}| - \frac{1}{|\tilde{\mathbf{n}}|} \right) \right] \tilde{T}_\alpha^p (\tilde{\mathbf{n}} \times \tilde{\mathbf{e}}_\alpha) \quad (80)$$

6. SOLUTION ALGORITHM

The solution algorithm of the present impact system is summarized as follows.

1. form the contact frame including possible contacting nodes at t_n
2. solve the governing equation (34), (43), (36) and (79) with the time integration scheme (28) by some iteration algorithm, e.g. Newton-Raphson procedure, and obtain the nodal position of the bodies at t_{n+1} .
3. calculate the energy increment $\Delta \pi_c$ from (62).
4. calculate the discrete contact velocity \mathbf{v}_c^p from (71), and (72), and obtain the nodal velocity at t_{n+1} from (63).

It should be noted that the contact frame is not necessary re-formed at each time step as described above. The contact frame at t_n obtained in the previous time increment $[t_{n-1}, t_n]$ can be used for the current increment. The re-formation is, however, recommended to avoid the missing of newly contacting nodes.

7. NUMERICAL EXAMPLES

In this section, three numerical examples are shown to demonstrate the performance of the proposed method. The first example is the Hertz impact of two cylinders, which evaluates its numerical accuracy. The second one is the impact of two free flying rings, which verifies the conservation property of the proposed method. The final one is the frictional impact between a ring and a strip, which verifies the convergence and conservation properties under friction. The calculated results of the first and the second examples are compared with those obtained from the classical master-slave method with conservation algorithm proposed in reference [31].

In the numerical results shown below, the nodal contact force at $t = t_n$ is evaluated by the averaged value of the midpoints of the time step containing t_n , i.e.

$$\bar{\lambda}^p(t_n) \equiv \frac{\bar{\lambda}^p(t_{n-1/2}) + \bar{\lambda}^p(t_{n+1/2})}{2} \quad (81)$$

where $\bar{\lambda}^p(t_{n+1/2})$ is identical with $\bar{\lambda}^p$ in the time period $[t_n, t_{n+1}]$, and $\bar{\lambda}^p(t_{n-1/2})$ is that in the previous time period $[t_{n-1}, t_n]$. The contact pressure is also evaluated by the similar formulation with $\mathbf{x}_p(t_{n+1/2}) \equiv [\mathbf{x}_p(t_n) + \mathbf{x}_p(t_{n+1})]/2$. The smoothing approximation proposed in reference [32] is used for the evaluation of the pressure distribution to suppress its oscillation [10, 32].

7.1. Hertz impact of two cylinders

Two identical elastic cylinders of non-dimensional radius $R = 4$ impact against each other with opposite velocities $v_o = 2$ as shown in Figure 8(a). Each cylinder has the following properties: the Young's modulus $E = 1000$, the Poisson's ratio $\nu = 0.2$, the thickness $h = 1$, and the mass density per unit area $\rho = 1$. This problem is identical with the impact problem of a cylinder and rigid foundation as shown in Figure 8(b). As in Figure 8(b), the cylinder is modeled by using four-noded nonlinear plane stress elements. The simulation is carried out with the time step width $\Delta t = 0.01$. In this case, the result is identical with that by the master-slave method because the frame is the surface line of the rigid foundation which is identical with the master segment used for the master-slave method.

The time histories of the total contact force F_c and the distance d_r between the centers of two cylinders are shown in Figure 9. The solution based on the Hertz static contact is also plotted in broken lines. The Hertz solution is calculated by solving the following differential equation [33, 34].

$$2\pi R^2 h \rho \ddot{d}_r = F_c \quad , \quad d_r = 2 \left[R - \frac{\eta F_c}{h} \left(\frac{2}{3} + \log \frac{Rh}{\eta F_c} \right) \right] \quad , \quad \eta = \frac{1 - \nu^2}{\pi E} \quad (82)$$

The Hertz solution assumes that the contact area is small and the inertial force is uniformly distributed in the cylinder. In other word, it does not consider the local oscillation within the cylinder. Therefore, the Hertz solution underestimates the contact force at the beginning of the impact when the inertia of the body near the contact surface increases the contact force. And it overestimates the contact force when the velocity of the center of the cylinder gets small. The total contact force for the present solution oscillates around $t = 0.65$, which is caused by the local vibration in the cylinders. Hertz solution cannot simulate such oscillation.

Figure 10(a) and (b) show the time history of the contact length a and the pressure distribution p along the horizontal axis s_1 when the approach of two cylinders is at maximum.

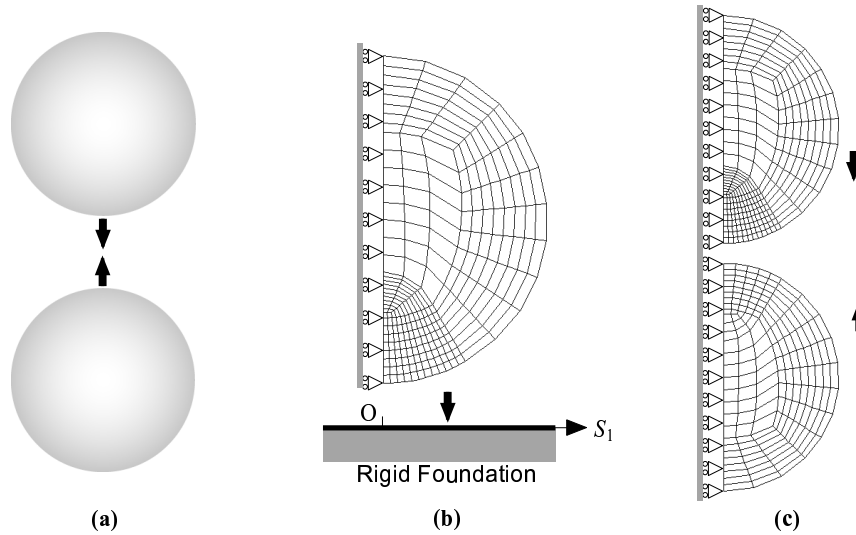


Figure 8. Hertz impact problem of two cylinders: (a) a schematic of the problem; (b) finite element model-1; and (c) finite element model-2

The Hertz solution of these two properties is given as Equation (83).

$$a = 4\sqrt{\frac{\eta R F_c}{h}} \quad , \quad p = p(s_1) = \frac{4F_c}{\pi a} \sqrt{1 - \left(\frac{2s_1}{a}\right)^2} \quad (83)$$

Because of the geometrical nonlinearity, the pressure at the center of the contact region is smaller than that of the Hertz solution whereas the pressure at the outer side is larger.

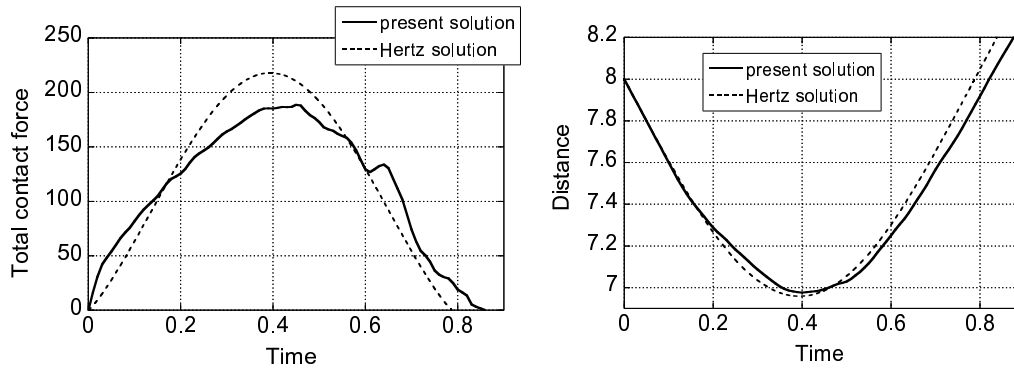


Figure 9. Hertz impact of identical cylinders (model-1): (a) total contact force; and (b) distance between centers of cylinders

In order to investigate the effect of nonmatch of the finite element (FE) mesh between two bodies, this problem is solved by using the FE mesh shown in Figure 8(c). The FE mesh of

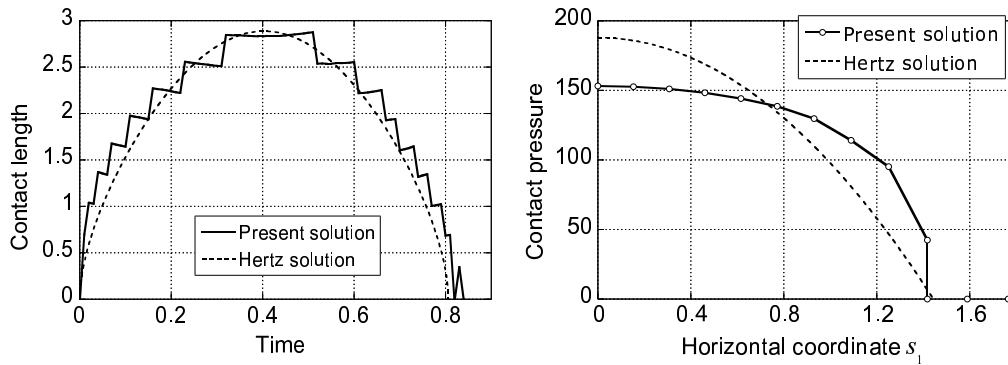


Figure 10. Hertz impact of identical cylinders (model-1): (a) contact length; and (b) contact pressure at the maximum approach

the lower cylinder is coarser than that of the upper cylinder. We call this FE model "model-2" whereas we call the model shown in Figure 8(b) "model-1". Figure 11 shows the time history of the total impact force and the contact pressure distribution along the horizontal axis. The difference between the model-1 and model-2 is little, which shows the present method is robust to nonmatch of the mesh. The difference between the present method and the master-slave method is also very little, which means that the present method can describe the pressure distribution without the laborious and sensitive construction of the pairs of master segments and slave nodes.

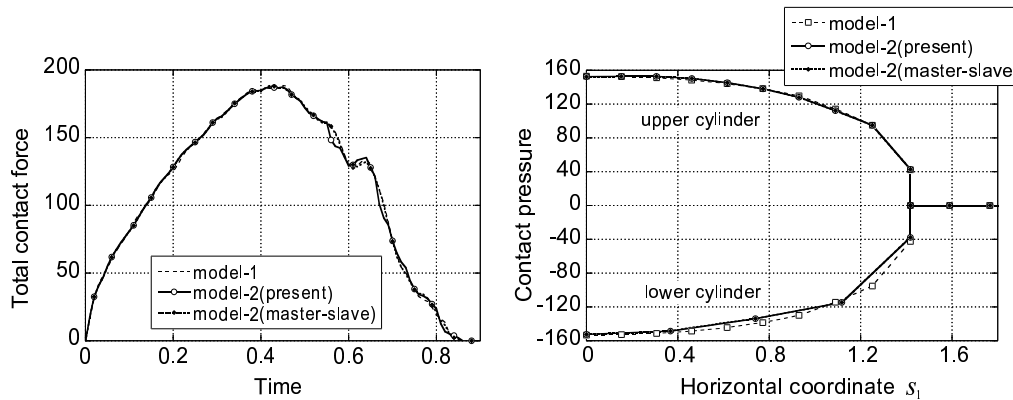


Figure 11. Hertz impact of identical cylinders (model-2): (a) total impact force and (b) contact pressure at the maximum approach

7.2. Impact of two free-floating rings

Two identical elastic ring of non-dimensional radius $R = 10$ impact against each other as shown in Figure 12. The initial coordinates of the center of Ring-1 and Ring-2 are $(0, 0)$ and $(20, 10)$, respectively. Ring-2 is initially at rest, and Ring-1 hits Ring-2 with the velocity $\mathbf{v}_o = (4, 0)$. Each ring has the following properties: the Young's modulus $E = 1000$, the Poisson's ratio $\nu = 1/6$, the thickness $h = 0.3$, and the mass density per unit area $\rho = 0.1$. This example is given in reference [31]. The number of the finite element division is 3 in radial direction. As in Figure 12, the division in the circumference direction is not uniform, but the possible contact region is much finer than the outer region. The total number of the division is 80. The time step width is $\Delta t = 0.01$.

Figure 13 illustrates the transient shape of the rings. Two rings are point-symmetric to each other. Figure 14(a) plots the total energy of the system and the energy stored in Ring-1. The difference of the energy of Ring-1 between the present and the master-slave method, ΔE_1 , is also plotted in Figure 14(a). The total angular momentum of the system and the angular momentum of Ring-1 are plotted in Figure 14(b). The difference of the angular momentum between two methods, ΔL_1 , is also plotted. The total energy and the angular momentum as well as the linear momentum are exactly conserved, and the difference between the present and the master-slave method is small. Figure 15 shows the pressure distribution and the ring configuration at $t = 0.92$, when the contact length is at maximum. The origin of the curvilinear coordinate s_1 is at the point of symmetry of two rings. The difference between the present and the master-slave method is small. When we employ the master-slave method to the impact problem in which the contact surface is curved, we should take great care of the determination of the contact pair so that no lack of the constraint nor overconstraint has occurs. If we fail the determination, the pressure distribution would be entirely wrong. On the other hand, the present method provides the necessary and sufficient number of frame nodes so that neither lack nor overconstraint occurs.

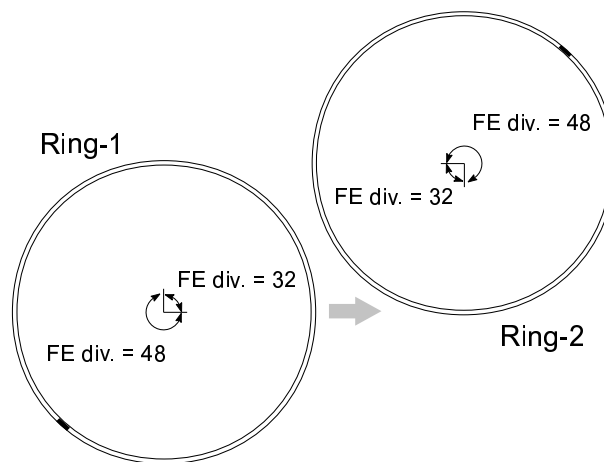


Figure 12. Impact of two rings: initial configuration

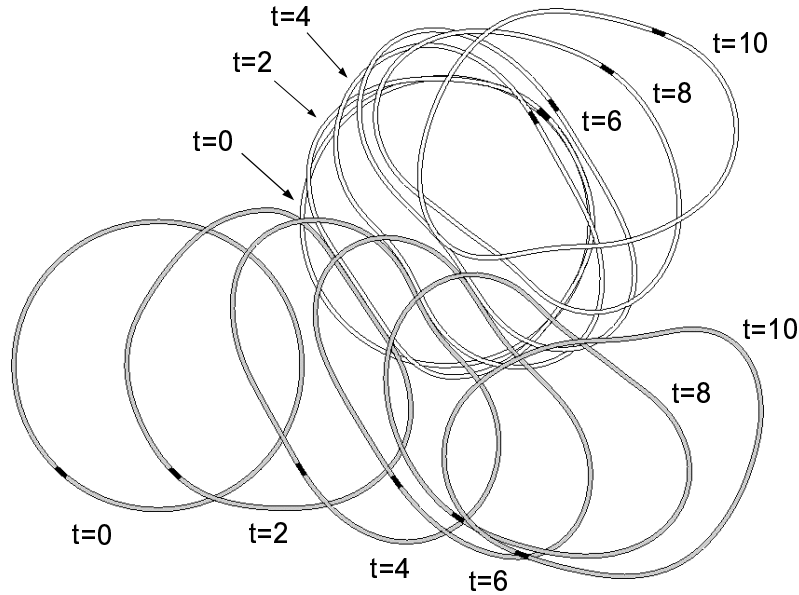


Figure 13. Impact of two rings: transient shape

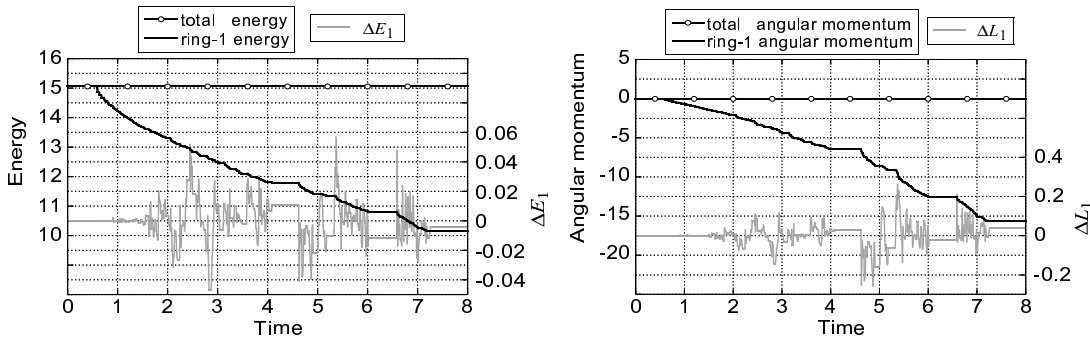


Figure 14. Impact of two rings: (a) energy; and (b) angular momentum

7.3. Impact of ring and strip

An elastic ring impacts against a thin elastic strip as in Figure 16. The radius and the thickness of the ring are $R = 0.29$ and $h_r = 0.2$, respectively. The length and the thickness of the strip are $L = 8$ and $h = 0.25$, respectively. They are made of same material with the following properties: the Young's modulus $E = 500$, the Poisson's ratio $\nu = 0.3$, and the mass density per unit area $\rho = 1$. The initial coordinate of the center of the ring is $(-3.125, 3.125)$, and that of the strip is $(0, 0)$. The strip is at rest initially, and the ring has the velocity $\mathbf{v}_o = (2, -1)$. The

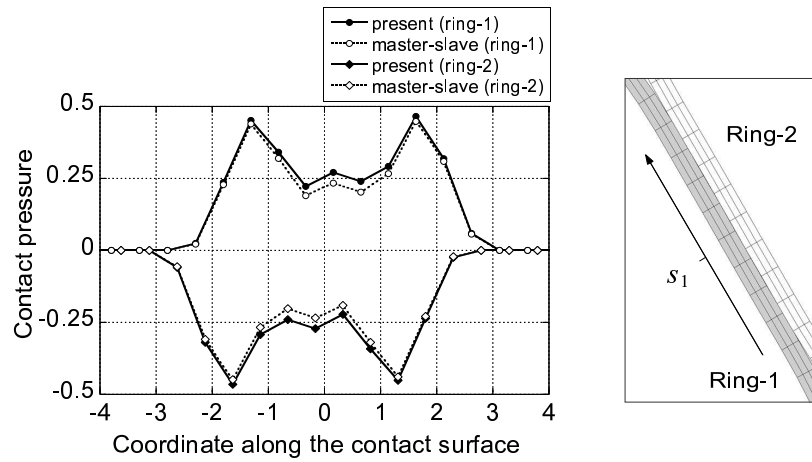


Figure 15. Pressure distribution at maximum contact length: (a) pressure distribution; and (b) ring configuration

number of finite element division of the ring is 48 in circumference and 3 in radial direction. That of the strip is 32 in longitude and 3 in thickness. The time step width is $\Delta t = 0.01$.

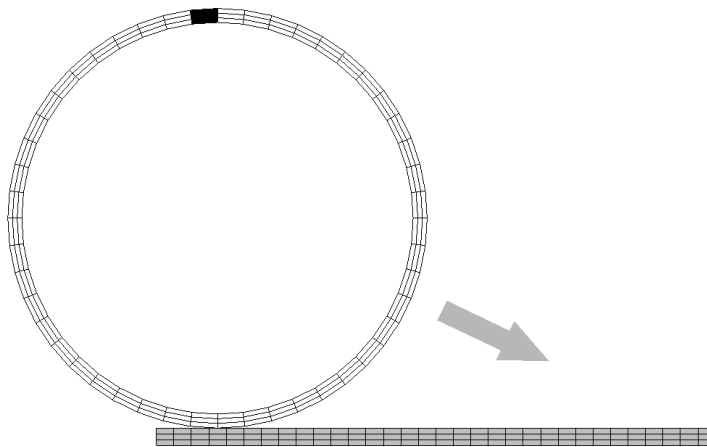


Figure 16. Frictional impact of ring and strip

Figure 17 illustrates the transient configuration in case of frictionless impact ($\mu = 0$) and that of frictional one with $\mu = 0.5$. In case of frictional impact, the ring trails the strip because of the frictional force. The time history of the stored energies is plotted in Figure 18(a), which shows the friction causes the high dissipation of the kinetic energy. The angular momentum of the total system and that of the ring in the frictional impact are plotted in Figure 18(b). The deviation of the total angular momentum from the initial value is also plotted in this

figure. This figure shows that the deviation of the total angular momentum is negligibly small even though the change of that of each body is large, so that the conservation of the angular momentum is almost satisfied in the present method. These results show the present method has no numerical difficulty to analyze the frictional impact problem.

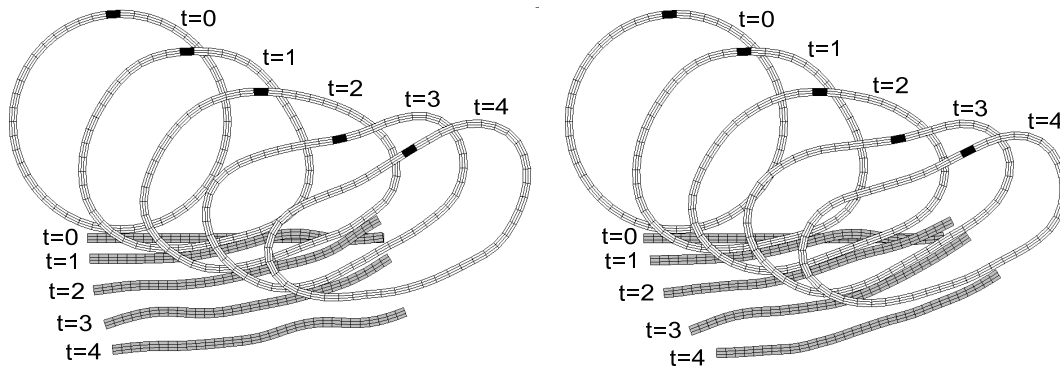


Figure 17. Transient configuration: (a) $\mu = 0$; and (b) $\mu = 0.5$

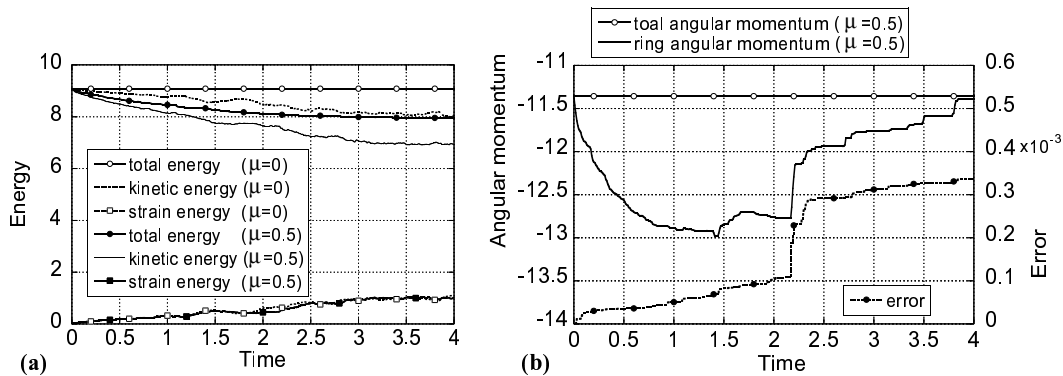


Figure 18. Impact of ring and strip: (a) energy; and (b) angular momentum ($\mu = 0.5$)

8. CONCLUSION

A formulation of the frictional impact system of elastic bodies is proposed. This method is based on the localized Lagrange multipliers technique. It introduces the contact frame in between the impacting bodies. The contact frame provides accurate prediction of the contact pressure as well as the total contact force and the deformation of the bodies without the laborious construction of the contact pairs that is needed in the classical master-slave method.

Furthermore, the modification from the frictionless impact problem to the frictional one is quite simple, and no numerical difficulty occurs in the simulation. The proposed method guarantees the conservation of the energy and the momentum in the frictionless impact, and the conservation of the linear momentum in the frictional impact. The conservation of the angular momentum in the frictional impact is approximately satisfied, and its error is negligibly small.

REFERENCES

1. Farahani K, Mofid M, Vafai A. A solution method for general contact-impact problems. *Computer Methods in Applied Mechanics and Engineering* 2000; **187**:69-77.
2. Stupkiewicz S. Extension of the node-to-segment contact element for surface-expansion-dependent contact laws. *International Journal for Numerical Methods in Engineering* 2001; **50**:739-759.
3. Crisfield MA. Re-visiting the contact patch test. *International Journal for Numerical Methods in Engineering* 2000; **48**:435-449.
4. Wang F, Cheng J, Yao Z. FFS contact searching algorithm for dynamic finite element analysis. *International Journal for Numerical Methods in Engineering* 2001; **52**:655-672.
5. Simo JC, Wriggers P, Taylor RL. A perturbed Lagrangian formulation for the finite element solution of contact problems. *Computer Methods in Applied Mechanics and Engineering* 1985; **50**:163-180.
6. Laursen TA, Simo JC. A continuum-based finite element formulation for the implicit solution of multibody large deformation frictional contact problems. *International Journal for Numerical Methods in Engineering* 1993; **36**:3451-3485.
7. Belgacem FB, Hild P, Laborde P. The mortar finite element method for contact problems. *Mathematical and Computer Modelling* 1998; **28**:263-271.
8. McDevittz TW, Laursen TA. A mortar-finite element formulation for frictional contact problems. *International Journal for Numerical Methods in Engineering* 2000; **48**:1525-1547.
9. Jones RE, Papadopoulos P. A novel three-dimensional contact finite element based on smooth pressure interpolations. *International Journal for Numerical Methods in Engineering* 2001; **51**:791-811.
10. Lei X. Contact friction analysis with a simple interface element. *Computer Methods in Applied Mechanics and Engineering* 2001; **190**:1955-1965.
11. Buscaglia GC, Durkn R, Fancello EA, FeijUo RA, Padra C. An adaptive nite element approach for frictionless contact problems. *International Journal for Numerical Methods in Engineering* 2001; **50**:395-418.
12. Heinstejn MW, Mello FJ, Attaway SW, Laursen TA. Contact-impact modeling in explicit transient dynamics. *Computer Methods in Applied Mechanics and Engineering* 2000; **187**:621-640.
13. Kloosterman G, von Damme RMJ, van den Boogaard AH, HuDtink J. A geometrical-based contact algorithm using a barrier method. *International Journal for Numerical Methods in Engineering* 2001; **51**:865-882.
14. Wriggers P, Krstulovic-Opara L, Korelj J. Smooth C1-interpolations for two-dimensional frictional contact problems. *International Journal for Numerical Methods in Engineering* 2001; **51**:1469-1495.
15. Coorevits P, Hild P, Pelle JP. A posteriori error estimation for unilateral contact with matching and non-matching meshes. *Computer Methods in Applied Mechanics and Engineering* 2000; **186**:65-83.
16. Chabrand P, Chertier O, Dubois F. Complementarity methods for multibody friction contact problems in finite deformations. *International Journal for Numerical Methods in Engineering* 2001; **51**:553-578.
17. Ricaud JM, Pratt E. Analysis of a time discretization for an implicit variational inequality modelling dynamic contact problems with friction. *Mathematical Methods in the Applied Sciences* 2001; **24**:491-511.
18. Czekanski A, Meguid SA, El-Abbasi N, Refaat MH. On the elastodynamic solution of frictional contact problems using variational inequalities. *International Journal for Numerical Methods in Engineering* 2001; **50**:611-627.
19. Rebel G, Park KC, Felippa CA. A contact formulation based on localised Lagrange multipliers: formulation and application to two-dimensional problems. *International Journal for Numerical Methods in Engineering* 2002; **54**:263-297.
20. Park KC, Felippa CA, Gumaste UA. A localized version of the method of Lagrange multipliers and its applications. *Computational Mechanics* 2000; **24**: 476-490.
21. Rebel G, Park KC, Felippa CA. A simple algorithm for localized construction of non-matching structural interfaces. *International Journal for Numerical Methods in Engineering* 2002; **53**:2117-2142.
22. Kikuchi N, Oden JT. *Contact Problems in Elasticity: a Study of Variational Inequalities and Finite Element Methods*. SIAM: Philadelphia, 1988.

23. Simo JC, Posbergh TA, Marsden JE. Stability of Coupled Rigid Body and Geometrically Exact Rods: Block Diagonalization and The Energy-Momentum Method. *Physics Reports* 1990; **193**:279-362.
24. Simo JC, Lewis DR, Marsden JE. Stability of relative equilibria I: The reduced energy momentum method. *Archive for Rational Mechanics and Analysis* 1991; **115**:15-59.
25. Simo JC, Posbergh TA, Marsden JE. Stability of relative equilibria II: Three Dimensional Elasticity. *Archive for Rational Mechanics and Analysis* 1991; **115**:61-100.
26. Simo JC, Wong KK. Unconditionally Stable Algorithms for Rigid Body Dynamics That exactly Preserve Energy and Momentum. *International Journal for Numerical Methods in Engineering* 1991; **31**:19-52.
27. Simo JC, Tarnow N. The discrete energy-momentum method. Conserving algorithms for nonlinear elastodynamics. *Journal of Applied Mathematics and Physics (ZAMP)* 1992; **43**:757-792.
28. Crisfield MA, Shi J. A Co-Rotational Element/Time-Integration Strategy for Non-linear Dynamics. *International Journal for Numerical Methods in Engineering* 1994; **37**:1897-1913.
29. Laursen TA, Chawla V. Design of energy conserving algorithms for frictionless dynamics contact problems. *International Journal for Numerical Methods in Engineering* 1997; **40**:863-886.
30. Demkowicz L, Bajer A. Conservative discretization of contact/impact problems for nearly rigid bodies. *Computer Methods in Applied Mechanics and Engineering* 2001; **190**:1903-1924.
31. Laursen TA, Love GR. Improved implicit integrators for transient impact problems - geometric admissibility within the conserving framework. *International Journal for Numerical Methods in Engineering* 2001; **53**:245-274.
32. Kikuchi BN, A smoothing technique for reduced integration penalty methods in contact problem, *International Journal for Numerical Methods in Engineering* 1982; **18**: 343-350.
33. Burr AH. *Mechanical Analysis and Design*. Elsevier Science, 1982.
34. Chandrasekaran N, Haisler WE, Goforth RE. Finite element analysis of Hertz contact problem with friction. *Finite Elements in Analysis and Design* 1987; **3**:39-56.